Influence of the mirror reflectance coefficient on the performance of the compound parabolic trough concentrator (CPC) : Numerical and experimental simulation in a Sahelian environment

Abstract

The objective of our study is to numerically and experimentally simulate the CPC operation according to three different values of the mirror reflectance coefficient. The study not only showed the importance of mirror reflectance in the performance of solar collectors but also estimated which of these three values fits well with the reality in the city of Ouagadougou. The thermal exchanges that took place in the CPC were presented. A matlab program was developed for the calculation and simulation of the different parameters of the solar concentrator. The differential equations governing the heat transfers in the different components of the device were discretized by the advanced finite difference method. They were solved by the Gauss-Seidel method. As for the experimental part, it consisted in the direct measurement of the global solar radiation, of the ambient temperature and of the fluid temperature by means of thermocouples placed on the different parts of the sensor. The experimental values are directly recorded with a datalogger. A statistical study was made using some indicators like coefficient of determination of R^2 , root mean square error (RMSE) and percentage of mean absolute error (MAPE). A validation of the obtained results by comparing the calculated values with the experimental values was presented. The results show that among the three values of the reflectance coefficient, the best results on the temperature of the fluid are obtained with the reflectance coefficient equal to 0.68 on the site of Ouagadougou.

Keywords: *CPC, Temperature, reflectance coefficient, simulation, statistical indicators.*

1. INTRODUCTION

Solar energy is the most abundant, the most geographically distributed and the most sustainable source of energy. Indeed, the sun delivers 885.106 TWh continuously to the surface of the Earth; that is 6,200 times the consumption of humanity in 2008. In other words, the sun brings to the Earth in less than one hour the energy consumed by humanity in one year [1-3]. The total energy of the oil reserves, estimated at 1.7.1022 J, would thus be compensated in only 1.5 days if the totality of the solar energy were used [2]. Although solar energy has been used by humans for millennia, electricity-generating technologies remained underdeveloped until the oil crisis of 1973, when solar energy experienced a significant resurgence of interest [1, 4]. Among the types of solar technologies, some are "concentrating" and use direct irradiance, such as Concentrating Solar Power (CSP) and Concentrated Photovoltaic (CPV), while the others are "non-concentrating" and use global irradiance, such as photovoltaic (PV) and planar solar thermal technologies[5]. CSP uses only direct sunlight, which is why the plants must be located in arid or semi-arid regions to benefit from significant direct radiation throughout the day and the year. Indeed, acceptable electricity production costs are for direct normal irradiation above 2000 kWh/m²/year. These values are typical of the "solar belt", i.e., located at latitudes below 40° north or south[6-7]. The Sahelian countries are the most suitable locations for the implementation of this technology. Burkina Faso, in particular, has a very high solar radiation potential capable of producing solar electricity. This average sunshine potential is estimated at 5.5 kWh/m^2/day for a sunshine duration varying from 3000 to 3500 h/year and an insolation of 8.3 hours per day[8]. This represents an unexploited energy source that could contribute to the reduction of its fossil energy bill. CSP technologies use mirrors to concentrate the solar energy that falls on the receiver. To fulfill their role, mirrors must maintain an essential functional property: reflectance. Reflectance plays a fundamental role in the performance of concentrating solar devices. There are three types of reflectance: hemispheric, diffuse and specular. Hemispheric reflectance integrates the intensity of the rays reflected in the hemisphere above the surface under consideration, i.e. the

total possible reflection [9]. When a beam of parallel rays encounters a rough or microstructured surface of size equal to or greater than the incident wavelength, each ray reaches a point on the surface with a different normal than the other points of incidence. Consequently, the angle of incidence and therefore the angle of reflection are specific to each ray, and the incident beam is reflected in all directions. This phenomenon is called diffuse reflectance [9]. For perfect specular reflectance, a beam of parallel rays would be reflected by a perfectly flat surface, i.e. with a roughness less than the wavelength of the beam. The reflected beam would then be composed of parallel rays, and the angle of incidence would be equal to the angle of reflectance regardless of the distance of the measurement from the reflecting surface [9].

In this paper, the heat exchanges that took place in the CPC were presented. A matlab program has been developed for the calculation and simulation of the different parameters of the solar concentrator. The differential equations governing the heat transfers in the different components of the device have been discretized by the advanced finite difference method. They were solved by the Gauss-Seidel method. As for the experimental part, it consisted in the direct measurement of the global solar radiation, of the ambient temperature and of the fluid temperature using J-type thermocouples. The experimental values are directly recorded with a datalogger. The fluid used for our experiment is water. Our work consists of a numerical and experimental simulation of the temperature of the fluid for three coefficients of reflectance of the mirror (rhom) of the parabolic trough concentrator (CPC) for four typical days of the year 2021 in the city of Ouagadougou. The aim is to determine among the three mirror reflectance coefficients (rhom =0.68, rhom =0.85 and rhom= 0.95) of the CPC the one whose fluid temperature seems to be close to the experimental reality. Theoretical and experimental results showed that the fluid temperatures of the three reflectance coefficients overestimate the experimental fluid temperature, however, the one where rhom =0.68 coincides with the experimental curve for the days of 06 and 20 April 2021. They point out that the theoretical curve with rhom=0.68 seems to be close with the experimental one.

2. MATERIALS AND METHODS

The experimental prototype is installed on the platform of the central maintenance workshop of the University of Joseph KI-ZERBO. The Figure 1 presents the photograph of the device designed to carry out the experimental study.
The descriptive diagram of the test bench is shown by Figure 2.

A data acquisition system "Midi logger GL200A" allows to collect up to 10 values simultaneously, these values are voltages expressed in volts. A calibration allows to convert the voltages in the unit of the measured values (°C). The data can be recorded on a computer or on a USB support. The values recorded by the acquisition system are then extracted in ".csv" format allowing their conversion and analysis on an Excel spreadsheet.

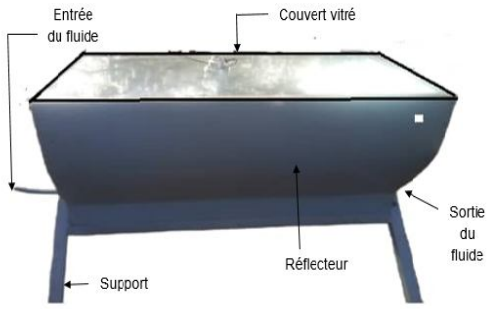

Fig. 1. Photo of the device

Data acquisition is programmed over a day with a time step of 5 minutes. The values obtained are used to calculate the temperatures. This finally allows drawing the curves of temperatures evolution by time.

The various tests carried out have started since 2017 during the period of strong sunshine in Burkina Faso from March to May of each year. The duration of the experimentation is 10 hours from 8:00 am to 06:00 pm. At the beginning of each experiment, the device is filled with water. There is no water circulation inside the collector because we have chosen a single daily filling boiler which is comfortable from the point of view of the control of the collector, but it is penalizing on a thermal plan because it increases a lot the hot surfaces which lose heat. Contrary to the boiler of smaller diameter which must be fed manually and several times during the day with a small pump, but which has less inertia and less losses; If the collector is used continuously, this intermittent supply temporarily lowers the temperature / pressure of the steam produced.

Verification is done by direct reading of the different temperatures on the data acquisition. At the end of the day the data acquisition is unloaded on a microcomputer where the digital data are recorded for the different treatments.

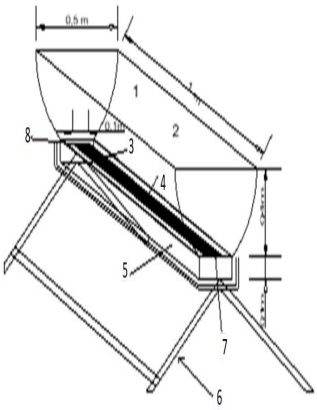

Legend
1: glass cover
2: reflector
3: absorber
4: internal glass
5: wooden frame
6: support
7: fluid inlet
8: fluid outlet

Fig. 2. The descriptive diagram of the experimental device

3. MODELING OF THE CPC

3.1. Simplifying Assumptions

The heat balance equations that will be established in the following are based on the following simplifying assumptions:

1. The flow is unidirectional and the regime is assumed to be transient;
2. The conditions are homogeneous on a section of the collector perpendicular to the flow;
3. Conduction in the glass is negligible;
4. The ambient temperature is the same at the front and at the back;
5. The air velocity and absolute humidity remain constant along the collector;
6. The thermophysical properties of the air depend linearly on the temperature;
7. The external and internal convective exchange coefficients are assumed to be constant over the entire length of the collector;
8. The fluid flow rate is assumed to be constant

3.2. The Heat Balance Equations of the Collector

3.2.1. At the canopy level

The glazed canopy receives direct and diffuse radiation on its upper surface and exchanges by convection and radiation with the surrounding environment [5].

$$M_c C_c \frac{\partial T_c(x,t)}{\partial t} = Q_c(x,t) + \left(h_{r,c-v} + h_{c,c-v}\right)(T_v - T_c) - h_{r,c-ciel}(T_c - T_{ciel}) - h_v(T_c - T_a) \quad (1)$$

3.2.2. At the glass level

In the same way, the energy balance for the glass is given by the relation (2) [5]:

$$M_v C_v \frac{\partial T_v(x,t)}{\partial t} = Q_v(x,t) + h_{r,p-v}(T_p - T_v) - h_{c,c-v}(T_v - T_c) - h_{r,c-v}(T_v - T_c) \quad (2)$$

3.2.3. At the absorber level

The energy balance at the absorber is obtained by expression (3) [5].

$$M_p C_p \frac{\partial T_p(x,t)}{\partial t} = Q_p(x,t) - h_{r,p-v}(T_p - T_v) - h_{c,p-f}(T_p - T_f) \quad (3)$$

3.2.4. At the fluid level

The energy balance for the heat transfer fluid circulating in the absorber tube is given by the relation (4) [10]:

$$\rho_f C_f e_f \frac{\partial T_f(x,t)}{\partial t} = -\frac{\dot{M}_f C_f}{l_p}\frac{\partial T_f(x,t)}{\partial x} + h_{c,p-f}(T_p - T_f) \quad (4)$$

3.3. Expressions of the Heat Transfer Coefficients

In order to draw up a complete balance of the transfers that took place in the concentrator, we must consider the flow mode of the fluid and the architecture of the device. In our study, we have neglected the heat transfer by conduction.

3.3.1. Heat transfer coefficients between the canopy and the exterior

We distinguish two types of heat exchange between the cover and the exterior: one by radiation and the other by forced and/or natural convection.

3.3.1.1. The coefficient of exchange by radiation between the canopy and the glass

The coefficient of exchange by radiation between the sky vault and the glass is given by the following expression:

$$h_{r,c-ciel} = k_B \varepsilon_c (T_c^2 + T_{ciel}^2)(T_c + T_{ciel}) \frac{A_c}{A_p} \quad (5)$$

3.3.1.2. The coefficient of exchange by convection due to wind

The exchange coefficient between the external environment and the glass is given by the formula of Mac Adams[11]:

$$h_v = (5.7 + 3.8V)\frac{A_c}{A_p} \quad (6)$$

3.3.2. The transfer coefficient between the cover and the glass.

There are two thermal exchanges between the glass and the cover. One by radiation and the other by convection.

3.3.2.1. The coefficient of exchange by

radiation between the cover and the glass

The coefficient of exchange by radiation between the cover and the glass is given by the following expression:

$$h_{r,c-v} = \frac{\sigma\varepsilon_c(T_c^2+T_v^2)(T_c+T_v)\frac{A_c}{Ap}}{\frac{1}{\varepsilon_v}+\frac{A_v}{A_c}(\frac{1}{\varepsilon_c}-1)} \quad (7)$$

3.3.2.2. The coefficient of exchange by convection between the cover and the glass

The convective transfer coefficient between the canopy and the glass is given by the relation (8) [12]:

$$h_{c,c-v} = (3{,}25 + 0{,}0085\frac{T_v-T_c}{2D_v})\frac{A_c}{A_p} \quad (8)$$

With:

$$D_v = \frac{2l_v(e_f+e_{p-v})}{l_v+e_f+e_{p-v}} \quad (9)$$

3.3.3. The transfer coefficient between the glass and the absorber

There is a heat exchange between the glass and the absorber. It is the solar radiation between the glass and the absorber. It is given by the following expression:

$$h_{r,p-v} = k_B\frac{(T_p^2+T_v^2)(T_p+T_v)}{\frac{1}{\varepsilon_p}+\frac{A_p}{A_v}(\frac{1}{\varepsilon_v}-1)} \quad (10)$$

3.3.4. The convection exchange coefficient between the absorber plate and the fluid

The heat transfer fluid exchanges heat by convection with the absorber. Correlations have been established for the calculation of the Nusselt number according to the nature of the fluid and the flow regime. In this study, the flow regime is laminar. For the calculation of the Nusselt number, the Mercier correlation is used [6]:

$$Nu_f = 4.9 + \frac{0.0606(R_eP_rD_h/L)^{1.2}}{1+0.0909(R_eP_rD_h/L)^{0.7}P_r^{0.17}} \quad (11)$$

With:

$$R_e = \frac{\dot{m}_fD_h}{l_pe_f\mu_f} \quad (12)$$

$$P_r = \frac{\mu_f}{\lambda_f}C_f \quad (13)$$

$$D_h = \frac{2l_pe_f}{l_p+e_f} \quad (14)$$

The convective exchange coefficient between the fluid and the absorber plate is given by the relation (15):

$$h_{c,p-f} = \frac{\lambda_f}{D_h}Nu_f \quad (15)$$

3.4. Expressions of Heat Quantities

3.4.1. The quantity of heat absorbed by the canopy.

It is given by the expression (16) [7]:

$$Q_c(t) = DNI\left[\overline{\alpha_c} + \overline{\alpha_c\tau_c}\zeta_m{}^{2<n>}\right]\frac{A_c}{A_p} \quad (16)$$

$$A_c = 2WL \quad (17)$$

$$A_p = L_pl_p \quad (18)$$

3.4.2. The quantity of heat absorbed by the glass

The quantity of heat absorbed by the glass is given by equation (19) [7]:

$$Q_v(t) = DNI\overline{\tau_c}\rho_m{}^{<n>}\overline{\tau_v}\left[\overline{\alpha_v} + \overline{\alpha_v\rho_v\rho_c}\zeta_m{}^{2<n>}\frac{A_v}{A_c} + \overline{\alpha_v}\overline{\zeta_p}\overline{\tau_v}\right]\frac{A_c}{A_p} \quad (19)$$

$$A_v = L_vl_v \quad (20)$$

3.4.3. The quantity of heat absorbed by the absorber plate.

Equation (21) gives the quantity of heat absorbed by the absorber plate [7]:

$$Q_p(t) = DNI\overline{\tau_c}\rho_m{}^{<n>}\overline{\tau_v}\left[\overline{\alpha_p} + \overline{\alpha_p\rho_v\rho_p}\frac{A_p}{A_v}\right]\frac{A_c}{A_p} \quad (21)$$

4. STATISTICS INDICATORS

Statistical indicators were used to determine the performance of these models. These statistical indicators are:

4.1. The coefficient of determination R^2

The indicator R^2 varies between 0 and 1, a value of 1 or close to 1 indicates a perfect agreement between the measured and calculated value, on the other hand a value close to 0 indicates a total disagreement.

$$R^2 = 1 - \frac{\sum_{i=1}^{k}\left(I_{ghm} - I_{ghc}\right)^2}{\sum_{i=1}^{k}\left(I_{ghm} - I_{ghmm}\right)^2} \quad (22)$$

4.2. The Mean Square Error (MSE)

The MSE is the arithmetic mean of the squares of the differences between model predictions and observations

$$\text{MSE} = \frac{1}{\text{K}}\sum_{i=1}^{K}\left(I_{ghm} - I_{ghc}\right)^2 \quad (23)$$

4.3. The root mean square error (RMSE)

The RMSE is a measure of the variation of the calculated values, according to each model around the measured values. The smaller the value, the better the model.

$$\text{RMSE} = \sqrt{\frac{1}{K}\sum_{i=1}^{K}\left(I_{ghm} - I_{ghc}\right)^2} \quad (24)$$

4.4. The Mean percentage Error (MPE)

The percentage of average error is given by the expression.

$$\text{MPE} = \frac{1}{K}\sum_{i=1}^{K}\left(\frac{I_{ghm} - I_{ghc}}{I_{ghm}}\right) \quad (25)$$

4.5. The mean absolute percentage error (MAPE)

It is given by the following equation:

$$\text{MAPE} = \frac{1}{K}\sum_{i=1}^{K}\left(\left|\frac{I_{ghm} - I_{ghc}}{I_{ghm}}\right|\right) \quad (26)$$

4.6. The Mean Error (ME)

The mean error gives an indication of the average deviation of the calculated values from the measured values. A positive value indicates an overestimation, while a negative value indicates an underestimation.

$$\text{MBE} = \frac{1}{K}\sum_{i=1}^{K}\left(I_{ghm} - I_{ghc}\right) \quad (27)$$

4.7. The mean Absolute Error (MAE)

It is obtained by the following relationship

$$\text{MABE} = \frac{1}{K}\sum_{i=1}^{K}\left(|I_{ghm} - I_{ghc}|\right) \quad (28)$$

5. THEORETICAL AND EXPERIMENTAL RESULTS

5.1. Theoretical results

The experimental curves were smoothed with a coefficient of determination of R^2 tending to 1 with Excel. The figure shows that the theoretical fluid and absorber temperatures are above the experimental temperatures. The both, theoretical and experimental curves have a bell-shaped curve whose peak is reached at solar noon and the minimum values are seen at sunrise and sunset. For the four days the evolution of the temperatures is the same, there is no difference in the slopes of the curves.

The results show that the temperature of the collector components depends on the incident solar flux and the surrounding climatic conditions. The theoretical fluid temperature reaches 125°C while the experimental fluid temperature oscillates between 107 and 108°C for an experimental global solar radiation up to 955 W/m^2 and a maximum ambient temperature of 43°C for the day of April 02, 2021.

Figure 3 below shows the theoretical fluid temperature curves obtained for four typical days in April 2021 for three different values of the mirror reflectance coefficient (rhom=0.68, rhom=0.85 and rhom=0.95). The different curves have a bell-shaped appearance. The peak is reached at solar noon and the low temperature values are obtained at sunrise and sunset. For the coefficients of reflectance 0.68, 0.85 and 0.95 the maximum values can reach respectively 120, 160 and 180 °C for the days of 02 and 09 April 2021 and 108, 120 and 150 °C for the days of 06 and 20 April 2021. It also appears that the higher the reflectance coefficient, the higher the temperature of the fluid. The reflectance coefficient of the mirror affects the operation of the CPC. The higher its value, the higher the temperature of the fluid becomes. The choice of reflectors is very important to obtain very high fluid temperatures.

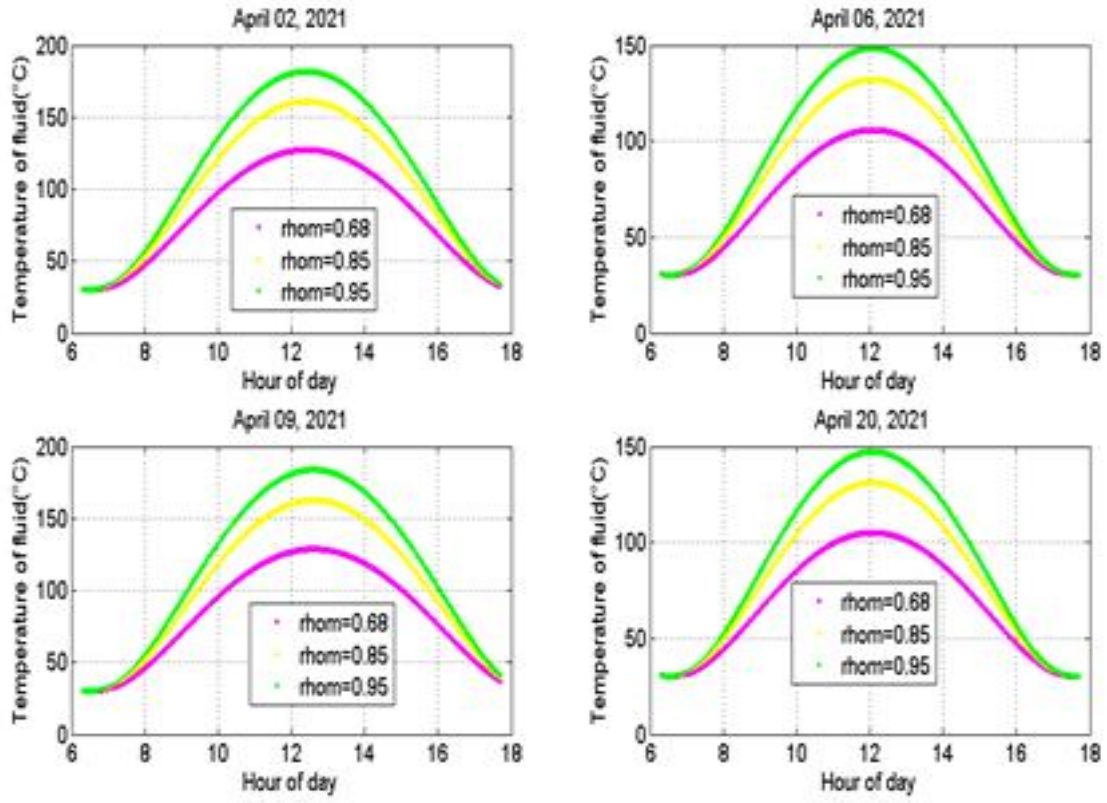

Fig. 3. Theoretical variations of the fluid temperature as a function of the time of day for four different days and for three different values of the reflectance coefficient. rhom=0,68, rhom=0,85 and rhom=0,95.

5.2. Comparison of theoretical results with experimental results

Figure 4 below shows the theoretical and experimental evolution of global solar radiation for four days in April. The pyranometer used for the measurement of solar irradiation during the experimental manipulations measures only the global solar radiation. The analysis shows that the theoretical solar radiation of the Eufrat model totally underestimates the experimental global solar radiation on a horizontal plane for the day of April 06, 2021 and for the other days the theoretical model underestimates the experimental curves from 10 hours. All theoretical and experimental curves have a bell shape. The minimum values are reached at sunrise and sunset and the maximum values at solar between 12:00 and 13:00. The maximum value of the theoretical global solar radiation is 812 W/m^2 against 955 W/m^2 for the experimental maximum value of the global solar radiation measured on the site on April 02 and 09, 2021. It is 700 W/m^2 against 825 W/m^2 on April 06 and 20, 2021. Figure 5 below shows the theoretical and experimental variation of the ambient temperature. The examination of this figure shows that the curves have the same shape. They take maximum values from 13 hours and minimum values at the first and last hours of the day. Figure 5 also shows that the theoretical ambient temperature of the Capderou model greatly overestimates the ambient temperature measured at the site. Referring to the day of April 06, 2021, the maximum measured ambient temperature is 43 °C against 42 °C the maximum theoretical value of the Capderou model at solar noon. The differences are perceptible at sunrise and sunset and are very small around solar noon. Figure 6 below shows the juxtaposition of the theoretical curves with the experimental fluid temperature curve. The smoothed experimental curve has the same shape as the theoretical curves of the fluid temperature. The theoretical curves overestimate those experimental for the days of 02 and 09 April 2021 and for the days of 06 and 20 April it tends to merge at some points with the theoretical curve whose reflectance coefficient is equal to 0.68.

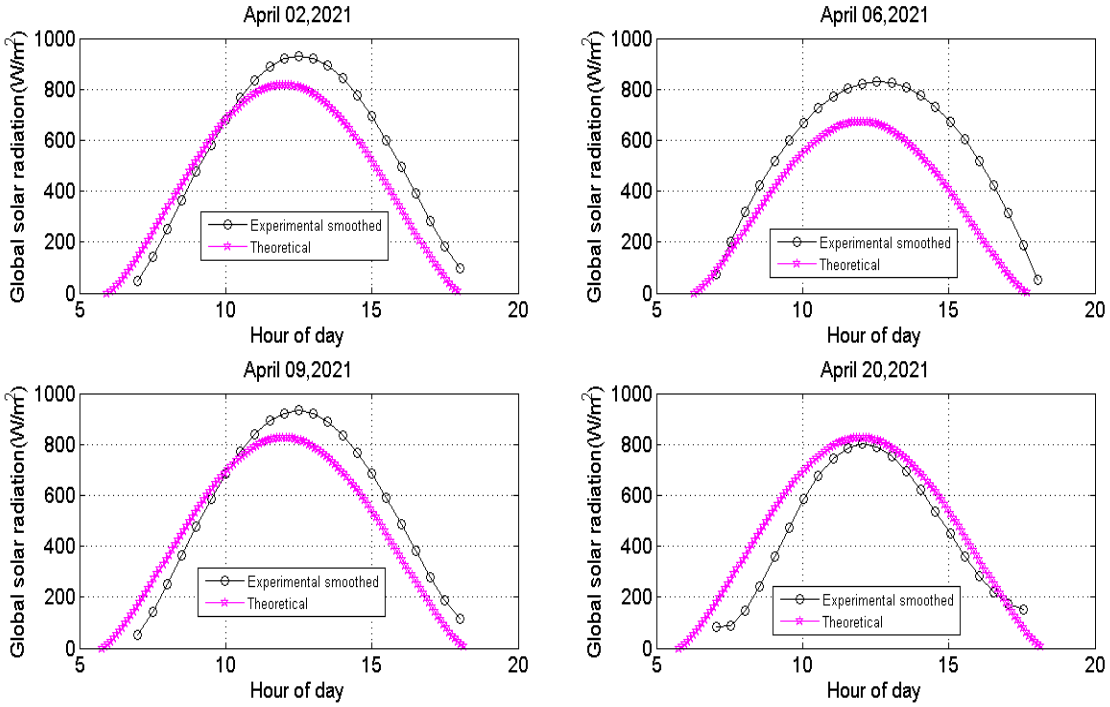

Fig. 4 : Theoretical and experimental evolution of global solar radiation for four days in April

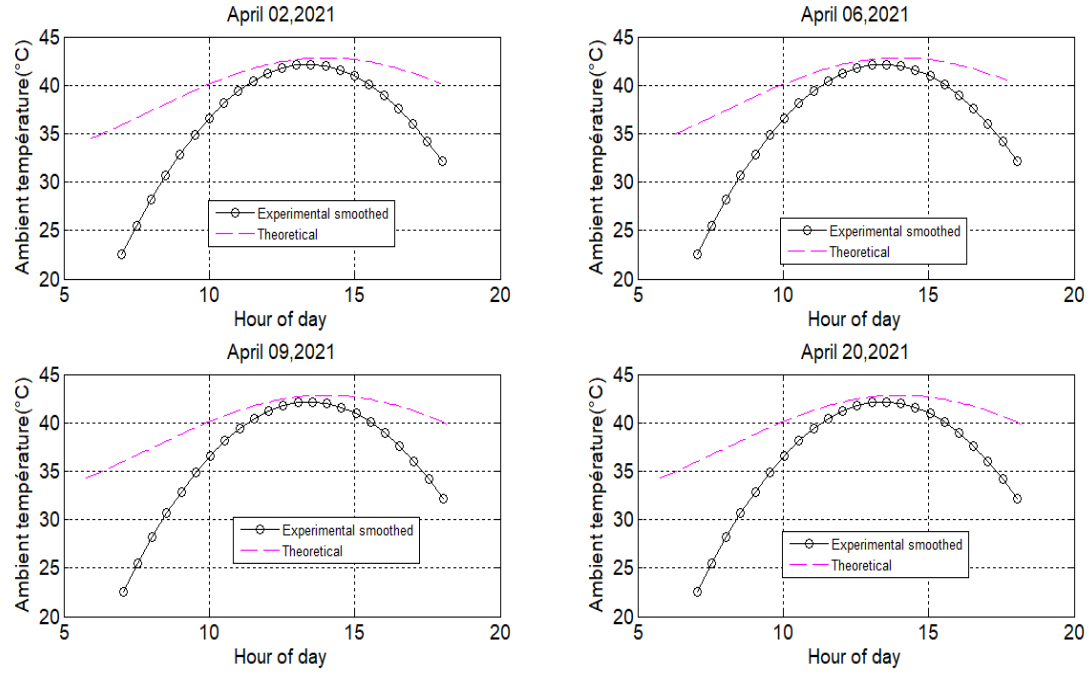

Fig. 5. Theoretical and experimental evolution of ambient temperature for four days in April

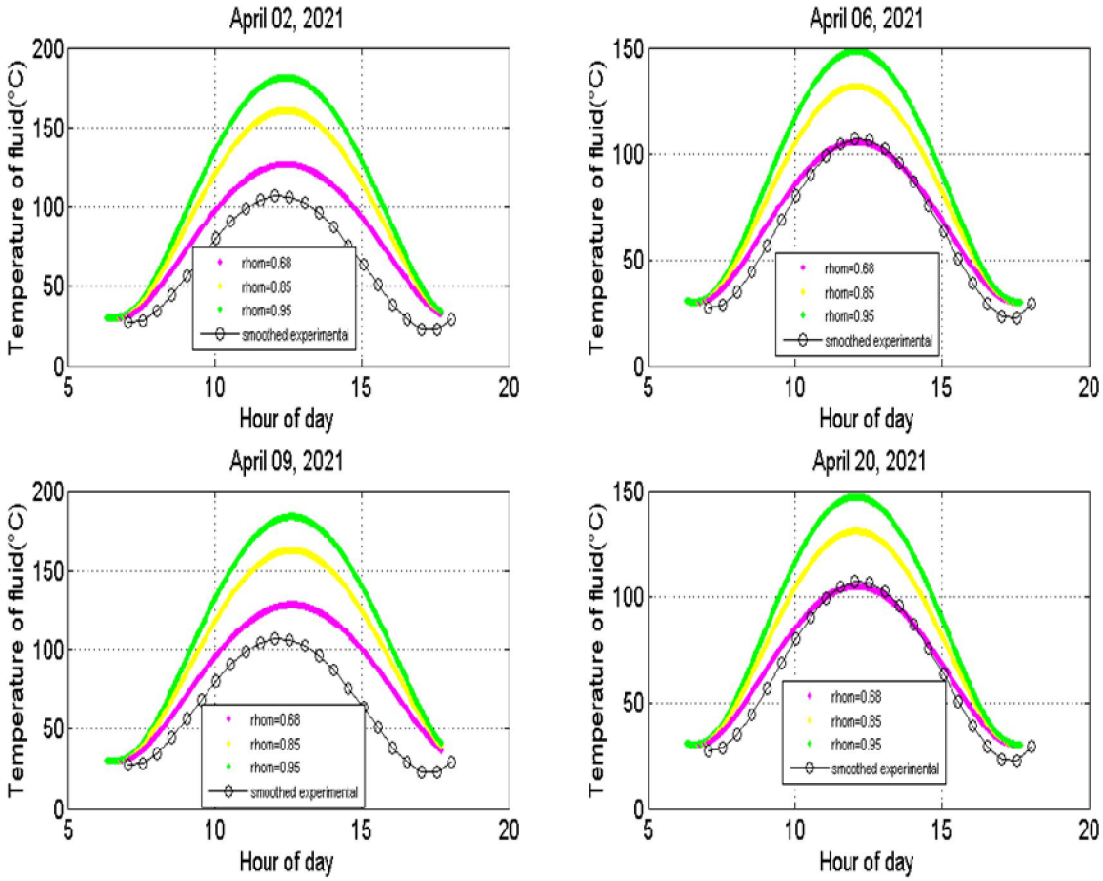

Fig. 6 . Theoretical and experimental variations of the fluid temperature as a function of the time of day for four different days and for three different values of the reflectance coefficient rhom=0,68, rhom=0,85 and rhom=0,95

5.3. Discussions

Aluminum-silver alloy as a commonly used reflector material has a reflectance of 0.97. However, its reflectance, if not properly protected, can decrease considerably due to tarnish in the atmosphere. On the other hand, the reflectance of aluminum, another commonly used reflective material, does not change much under atmospheric conditions. However, its reflectance is not as high as that of silver. Therefore, in order to achieve desirable characteristics for solar reflectors made of silver or aluminum, and to reach a reasonable compromise, aluminum-silver alloy films (first prepared by Harris and Siegel in 1948) were used as solar reflectors overcoming the problem of silver corrosion, although not as high a reflectance as silver. The reflectance of these alloys is between 0.6 and 0.8[13].

It should be noted that although silver mirrors have a higher reflectance than aluminum mirrors, to obtain a good silver mirror, five layers would be required whereas aluminum mirrors would require only two layers i.e., an aluminum film and a protective clear film; also, there is less corrosion on aluminum mirrors than on silver mirrors because the adhesion to the glass of aluminum mirrors is better and tarnishing due to sulfide does not occur[14]. Reflectors with a coefficient of 0.6 give fluid temperatures that are close to our experimental results.

For some days, the theoretical and experimental curves seem to merge. The maximum temperature reached by our device at solar noon with this reflectance coefficient is between 105 and 110°C depending on the solar radiation of the day. R. Almanza (1992) has developed a type of aluminum solar mirrors by integrating first and second surface aluminum mirrors i.e. glass/Al/SiO2/Al/. The reflectance of the mirrors is 0.85-0.86[14].

By integrating this reflectance coefficient in our numerical simulation program, the maximum fluid temperature varies between 140 and 160°C at

solar noon. This range of fluid temperature overestimates the experimental values of fluid temperatures that we measured. Mirror reflectance enhancing double layers (MgF_2 + CeO_2, Al_2O_3 + TiO_2, and SiOx + TiO_2) were used in a study by G. Hass (1982) to increase the reflectance of aluminum mirrors. These types of reflectors have reflectance coefficients greater than 0.90 [15]. The numerical simulation with this type of reflector in our case offers a temperature range of 150 to 180 °C. These temperatures are well above the temperatures measured experimentally at our experimental site.

5.4. Validation of the CPC model

Tables 1, 2 and 3 below present the results of statistical calculations of some indicators between the theoretical results obtained for three (03) different values of the reflectance coefficient and the experimental data of the fluid temperature for four days. We note that the higher the reflectance coefficient, the higher its temperature. Similarly, the theoretical curves largely exceed the experimental curves except for the days of 06 and 20 April 2021 where for rhom=0.68 the curves seem to merge at some points with those experimental. The experimental trend curves and the theoretical curves for the rhom values (rhom=0.68, rhom=0.85, m=0.95) show discrepancies. Comparison of the estimated values with the measured values generally shows that all three models give an overestimation of the calculated values.

Among the three theoretical models, we find that the one with rhom=0.68 has the highest R^2 values and the lowest MSE, RMSE, MPE, MAPE, ME and MAE values. The negative R^2 values are divergent values. Statistical analysis based on the coefficient of determination of R^2, root mean square error (RMSE) and percentage of mean absolute error (MAPE) shows that for the four days the coefficients of determination of R^2 for rhom=0.68 are close to 1 so this theoretical model is the best model to estimate the reality. Moreover, the RMSE values are the lowest compared to the other values of rhom=0.85 and rhom=0.95. Regarding the percentage of the mean absolute error (MAPE), the percentages of the model where rhom=0.68 are less than or equal to 14%, i.e. the difference between the theoretical temperature and the experimental one is 14%, whereas for the other theoretical models the percentages of the mean absolute error are higher than 14%.

It is found that among the three proposed models, the best results are those obtained with rhom=0.68. So we validate the theoretical model of the CPC by considering rhom=0,68.

Table 1: The results of statistical calculation for rhom =0.68.

Date	R^2	MSE	RMSE	MPE	MAPE	ME	MAE
02/04/2021	0,78	171,52	13,10	-0,11	0,12	-9,33	9,33
06/04/2021	0,78	200,46	14,16	0,12	0,14	10,69	10,69
09/04/2021	0,80	159,16	12,62	-0,13	0,13	-9,82	9,82
20/04/2021	0,82	152,18	12,34	0,02	0,15	3,06	9,94

Table 2: The results of statistical calculation for rhom =0.85.

Date	R^2	MSE	RMSE	MPE	MAPE	ME	MAE
02/04/2021	-0,51	1296,44	36,01	-0,37	0,37	-27,90	27,90
06/04/2021	0,54	154,14	12,42	-0,04	0,13	-3,45	9,86
09/04/2021	-3,22	3876,22	62,26	-0,56	0,57	-34,79	34,94
20/04/2021	0,71	252,81	15,90	0,00	0,16	-2,30	12,24

Table 3: The results of statistical calculation for rhom =0.95.

N° du jour	R2	MSE	RMSE	MPE	MAPE	MBE	MABE
02/04/2021	-1,61	2243,89	47,37	-0,49	0,49	-38,78	38,78
06/04/2021	-3,49	3859,28	62,12	-0,62	0,67	-28,73	32,23
09/04/2021	-2,05	2616,19	51,15	-0,56	0,56	-42,00	42,00
20/04/2021	0,21	682,45	26,12	-0,21	0,27	-16,64	20,56

6. CONCLUSION

In this paper, we proposed to do numerical and experimental simulation of the fluid temperature for three CPC mirror reflectance coefficients. Theoretical and experimental methodology was done Statistical analysis was also done by employing coefficient of determination of R^2 , mean square error (MSE), root mean square error (RMSE) ,, percent mean error (MSE), percent mean absolute error (MAPE), mean error (ME) and mean absolute error (MAE). The results showed that the reflectance coefficient of the mirror influences the operation of the CPC. The higher its value, the higher the temperature of the fluid becomes. It also appears that among the three coefficients, the best results on the fluid temperature are obtained by the reflectance coefficient equal to 0.68 on the Ouagadougou site, the other coefficients overestimating the experimental values of the fluid temperature. The choice of reflectors remains essential to obtain very high temperatures of the fluid.

7. REFERENCES

1. Avenel, C., Durabilité des miroirs pour l'énergie solaire à concentration : étude des modes de vieillissement. 2018, Matériaux .Université Clermont Auvergne [2017-2020].Français. ffNNT: 2018CLFAC035
2. G. W. Crabtree, N.S.L. and Solar energy conversion. Physics Today, 2007. vol. 60 (3), pp. 37 – 42.
3. (IEA), I.E.A., Technology roadmap - solar thermal electricity. 2014.
4. R. Girard, Rapport d'activité : Etude de la durabilité des miroirs CSP, Commissariat à l'Énergie Atomique et aux Énergies Alternatives (CEA). 2014.
5. International Energy Agency (IEA), Solar Energy perspectives 2011. Renewable Energy Technologies, 2011.
6. A. Fernandez-Garcia, E.Z., L. Valenzuela, and M. Perez, , Parabolic-trough solar collectors and their applications. Renewable and Sustainable Energy Reviews, 2010. vol. 14, no. 7, pp. 1695 – 1721.
7. L. A. Weinstein, J.L., B. Bhatia, D. M. Bierman, E. N. Wang, and G. Chen, , Concentrating solar power. Chemical Reviews, 2015.
8. AZOUMAH Y, e.a., Siting guidelines for concentrating solar power plants in the Sahel: Case study of Burkina Faso. Solar Energy, 2010. 84:1545–53.

9. S. Meyen, M.M., C. Kennedy, G. Zhu, M. Gray, J. Crawford, S. Hiemer, W. Platzer, A. Heimsath, M. O'Neill, S. Ziegler, S. Brändle, and A. Fernández,, Parameters and method to evaluate the solar reflectance properties of reflector materials for concentrating solar power technology. tech. rep., SolarPACES workgroup, 2013.
10. R.Tchinda, solved the governing equations of the energy to predicted the performance of air heater collector with the CPC having an absorber with flat plate. 2008.
11. DUFFIE. J. A., B.W.A., Solar engineering of thermal processes, ed. é. 2nd. 1991, Wiley.
12. Hsieh, C.K., Thermal analysis of CPC collectors. Elsevier Ltd, January 1981, Department of Mechanical Engineering, University of Florida
13. ADAMS, C., et al., Co-sputtering of aluminum-silver alloy mirrors for use as solar reflectors.Thin Solid Films. 1979: p. 63,151–154.
14. ALMANZA, R., et al., Advances on aluminum first surface solar reflectors. SPIE, 1992.
15. HASS, J., et al., Reflectance and preparation of front surface mirrors for use at various angles of incidence from the ultraviolet to the far infrared Phys. Thin Films,12, 1982: p. 1–49.

8. NOMENCLATURE

Dimensioned numbers
Gr: Grashoff number
Nu: Nusselt number
Pr: Prandtl number
Re: Reynolds number
Greek letters
α: The absorption coefficient
ε: The emissivity
ζ: The reflectance coefficient
η: The efficiency of the concentrator
ϑ: The density, kg m^{-3}
ρ: The specific heat, J kg^{-1} K^{-1}
τ: The transmission coefficient
Latin letters
A: Surface area, m_2
C: The heat capacity, J kg^{-1} K^{-1}
e_f : The distance between the bottom of the collector and the absorber plate,
e_{p-v} :The space between the absorber plate and the glass, m
h: The transfer coefficient, Wm^{-2} K^{-1}
l: The width, m
L: The latent heat of vaporization, J kg^{-1} K^{-1}
M: The mass of the body, kg
M ': The mass flow rate, kg s^{-1}
n: The average reflection number
P: The pressure, bar
Q: The quantity of heat absorbed, J
T: The temperature, °C
V: Wind speed, m/s
Indexes
c: Covered
c,c-v: Convective between the cover and the glass
c, p-f: Convective between the absorbing plate and the fluid
f: Fluid
fe: Finale
ie: Initiale
p: Absorbing plate
v: Glass
u: Useful